PROCEEDINGS, Thirty-Eighth Workshop on Geothermal Reservoir Engineering
Stanford University, Stanford, California, February 11-13, 2013
SGP-TR-198

STRESS ANALYSIS FOR BOREHOLES ON DEPARTMENT OF DEFENSE LANDS IN THE WESTERN UNITED STATES: A STUDY IN STRESS HETEROGENEITY

Kelly Blake

Navy Geothermal Program Office
429 Bowen Road, Stop 4011
China Lake, CA 93555
Email: kelly.blake@navy.mil

ABSTRACT

Image logs from boreholes drilled by the Navy Geothermal Program Office (GPO) at five geothermal areas in the western United State (Fallon Naval Air Station, NV, Hawthorne Army Depot, NV, Coso Geothermal Field, Naval Air Weapons Station China Lake, CA, Chocolate Mountains Aerial Gunnery Range, CA (Marine Corps Air Station, Yuma, AZ) and Naval Facility El Centro, CA) were analyzed to identify natural fractures intersecting the borehole, to determine the stress field acting on fractures proximal to the borehole and to quantify the amount of stress heterogeneity with depth. Horizontal principal stress orientations vary on the multiple kilometer scale largely due to the structural setting, but seem to vary at the meter and centimeter scale in the studied boreholes due to slip on fractures proximal to the hole, intersected lithology and, in highly stressed environments, slip on large regional faults. The average maximum horizontal principal stress orientation, revealed by induced structures in the studied boreholes, range from an azimuth of 081° to 133° and the standard deviations in stress orientation has a range of 11° to 46°. Spectral analysis was used to determine the variation of principal stress orientation from a calculated vertical axis. This analysis yields a linear spectral slope for each borehole, which was then compared to earthquake frequency and magnitude data and lithologic data from Gamma Ray logs to determine the control on stress variation. The amount of standard deviation and the linear spectral slope determines the stress heterogeneity for each of the studied boreholes. A high variation of principal stress orientation suggests a greater number of optimally oriented fractures to transmit fluid and thus a greater opportunity to intersect fluid pathways.

INTRODUCTION

Exploration at the Navy GPO begins with basin geological analyses-geology, geochemistry, geophysics, shallow temperature probes, 500 foot temperature gradient holes and then a deeper geophysical test hole is drilled. Geophysical image logs are collected for the purpose of determining the density of fractures the borehole intersects and the apparent aperture of the fractures to better understand the variation in lithology with depth, determine potential fluid entries and to gain a better understanding of the stress state in the vicinity of the drilled borehole. This study utilizes Ultrasonic Borehole Imager (UBI), Formation Micro-Scanner (FMS) and ABI85 Acoustic Borehole Televiewer (BHTV) from the Fallon Naval Air Station (NAS), Fallon, NV, Hawthorne Army Depot (HWAD), Hawthorne, NV, Coso Geothermal Field, Naval Air Weapons Station (NAWS), CA, Naval Facility El Centro (NAFEC), CA and Chocolate Mountain Aerial Gunnery Range (CMAGR), CA (Marine Corps Air Station, Yuma, AZ) (Figure 1).

Figure 1: Locations of the studied test holes within Department of Defense lands that span multiple tectonic regions.

The image logs analyzed span multiple stress regimes, tectonic environments and lithologies from the Basin and Range (Fallon and Hawthorne, NV) through the Eastern California Shear Zone (Coso, CA) to the Salton Trough (Chocolate Mountains and Superstition Mountains, CA). The variation in horizontal principal stress orientation occurs between the analyzed sites and within sites. By comparing the stress data to the differences in exploration site, it should then be feasible to determine the cause of stress heterogeneity with depth, how this understanding can aid the further exploration of a possible resource and try to figure out how the stress heterogeneity may control the movement of fluids at depth.

Multiple scale variation in stress orientation can be seen in borehole image log analysis, focal mechanisms (e.g., World Stress Map, 2008; Heidbach et al., 2010), in-situ stress measurements (e.g., Hickman et al., 2002; Davatzes and Hickman, 2009), fault slip data (Belier and Zoback, 1995), alignments of volcanic structures (Zoback, 1989) and geodetic measurements of strain (Bennett et al, 2003; Hammond and Thatcher, 2005; Kremer et al., 2009; 2010), but smaller scale variation (meter to centimeter) also occurs throughout the brittle crust (Day-Lewis et al., 2010; Valley and Evans, 2011; Blake and Davatzes, 2011; 2012). In geothermal reservoirs, the stress state, and therefore the variation in stress state, can aid in the exploration of geothermal reservoirs (Curewitz and Karson, 1997; Davatzes and Hickman, 2006; Faulds et al., 2006), the placement of future boreholes (Barton et al., 1997; Heffer, 2002), can control the connectivity of fractures and thus movement of fluid (recharge or injection) at depth (Heffer 2002).

GEOLOGIC SETTINGS

Fallon, NV is located in the Basin and Range Province and at the northern edge of the Eastern California Shear Zone. These regions are both associated with normal faulting with localized strike slip movement, a thinning of the brittle crust and shallow high heat flow (Hill, 1971; Eaton, 1982). Test holes FOH-3D and FLTH 88-24 were drilled by the Navy GPO on NAS Fallon and both are drilled into inter-bedding lake sediments at shallow depths and then andesite flows and ash flow tuffs. FOH-3D is drilled to a depth of 2743 meters (~9000 feet) and FLTH 88-24 is drilled to 1524 meters (5000 feet); the volcanic

bedrock is intersected at 701 meters (~2300 feet) and 884 meters (~2900 feet) respectively. The Carson Sink is an area of active WNW-ESE extension of ~1 mm/year determined through GPS studies (Faulds et al., 2006; Hammon and Thatcher, 2005) with local variation in the direction of displacement (Hammond et al., 2007; Blewitt et al., 2009; Kremer et al., 2010).

Hawthorne, NV is within the Walker Lane in the southwestern corner of the area surrounding Walker Lake basin, which is bounded by the Wassuk Range to the Garfield Hills. The Walker Lake basin is an asymmetric half-graben that has numerous normal faults with connecting strike slip faults (Shoffner et al., 2010). The geophysical test hole HWAD-2A was drilled on HWAD to a depth of 1433 meters (~2700 feet) and intersected alluvium above fractured granite at 274 meters (900 feet). HWAD-3 was drilled northeast of HWAD-2A, and on the hanging wall of a normal fault, to a depth of 1219 meters (4000 feet) through alluvium into diorite at 1097 meters (3600 feet). The extension throughout this basin moves at varying rates, which when combined with the high strain rates suggests probable permeability in this area along well oriented fractures (Katzenstein et al., 2002; Moeck et al., 2010).

The Coso Geothermal field is located east of the Sierra Nevada Mountains within the Eastern California Shear Zone (Adams et al., 2000; Fialko and Simons, 2000; Wicks et al., 2001; Davatzes and Hickman, 2006; Davatzes and Hickman, 2010) and is located entirely within NAWS China Lake. The tectonic environment varies from normal faulting to strike-slip faulting with normal faulting in the Eastern California Shear Zone (Lin and Stein, 2004). Test hole 66-8 was drilled to 3165 meters (10385 feet) and intersects ash-flow sediments, then fractured granite and granodiorites at depth (Adams et al., 2000; Manley and Bacon, 2001; Wicks et al., 2001; Kovac et al., 2005). The high rates of shallow seismicity in this field suggest a shallow brittle-ductile transition and WNW-ESE extensional strains are inferred from focal mechanism inversions (Unruh and Steig, 2004; Monastero et al, 2005).

The NAFEC geophysical test hole NAFEC-3, is located on the north eastern side of the Superstition Mountains to the southwest of the Salton Sea. NAFEC-3 was drilled to a depth of 1067 meters (3500 feet) and intersected lakebed sediments, sandstone and conglomerate over a granodiorite basement. The right lateral Superstition Mountain fault trace to the west of the studied borehole demonstrates recent movement in InSAR images from this area (Bjornstad et al., 2006; Eneva personal communication). The borehole also lies along the western edge of a magnetic anomaly trending to the northwest (Shoffner personal communication) and in an area of historically active seismicity (Shearer et al., 2005; Haukksson and Shearer, 2005).

The CMAGR test hole 17-8 is located east of the Salton Sea, close to the terminus of the San Andres Fault. This test hole was drilled to 915 meters (3000 feet) through alluvium and then granodiorites at depth. The Salton Trough is an area of a great amount of tectonic activity including extension in the southeast-northwest direction, with significant associated seismicity and has shallow high heat flow due to rifts and mafic intrusions (Crowe et al., 1978; Alm et al., 2010). The excavation of the Mesquite gold mine southeast of the prospect area identified gold deposited along right-lateral strike-slip fractures that had a dilational component (Willis and Tosdal, 1992).

IMAGE LOG

Methods

Images of the borehole wall from the analyzed holes were created by measurements of electrical resistivity, acoustic reflections or sonic data to identify natural fractures, bedding/foliation and deformation of the borehole wall. The Formation Micro Scanner (FMS) measures the resistivity of the borehole wall through pads of electrode arrays at a constant electrical potential pressed against the borehole wall (Ekstrom et al., 1987), ALT's ABI85 Borehole Televiewer collects both the two way travel time and the amplitude of an acoustic pulse from the tool reflected by the borehole wall (Zemaneck et al., 1970) and the Ultrasonic Borehole Imager (UBI) uses a transducer to create a sound pulse; the tool then measures the amplitude and travel time of that pulse to create an image of the borehole wall (Brie et al., 1998).The natural fractures and deformation of the borehole appear as lower resistivity areas in FMS and scatter of the acoustic pulse in BHTH and UBI data; however the differences in the geophysical properties between the\logging tools and the quality of the image themselves had to be taken into account while analyzing these data and the eventual comparison of the data (Figure 2).

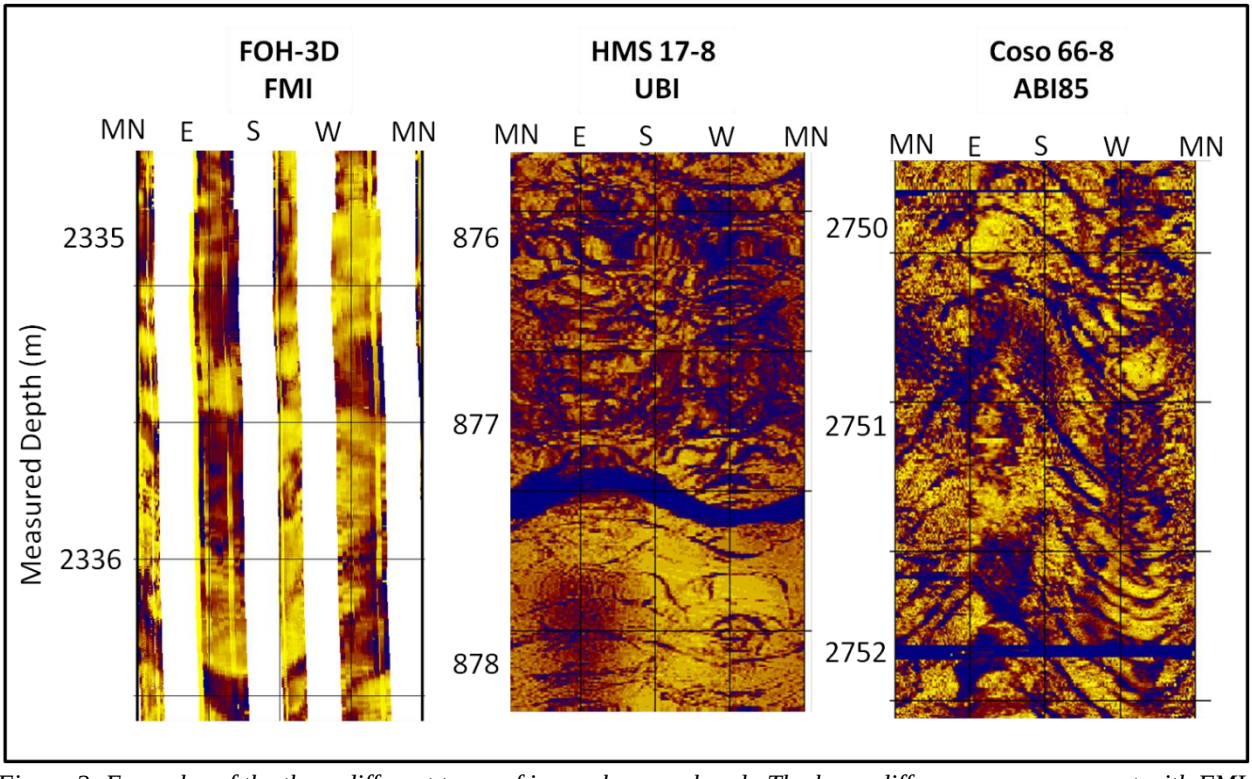

Figure 2: Examples of the three different types of image logs analyzed. The large differences are apparent with FMI data not covering the entire borehole, unlike both the UBI and ABI. In all three examples natural fractures with some degree of dip are seen in the image as sine waves.

The deformation of the borehole wall (borehole induced structures) identified in the studies holes were tensile fractures, petal-centerline fractures and breakouts. This failure of the borehole wall records the local orientation of the horizontal principal stresses (Zoback et al., 1985; Shamir and Zoback, 1992; Barton et al., 1997; Barton et al., 1998; Barton and Zoback, 2002). The concentration of normal stress acting tangentially to the borehole enhances compression or tension which results in breakouts or tensile fractures respectively occurring 180 degrees apart. Due to a concentration of stress below the drill bit as the borehole is being drilled, petal-centerline fractures form (Li and Schmidt, 1999; Davatzes and Hickman, 2010; Garza-Cruz and Davatzes, 2010) (Figure 3).

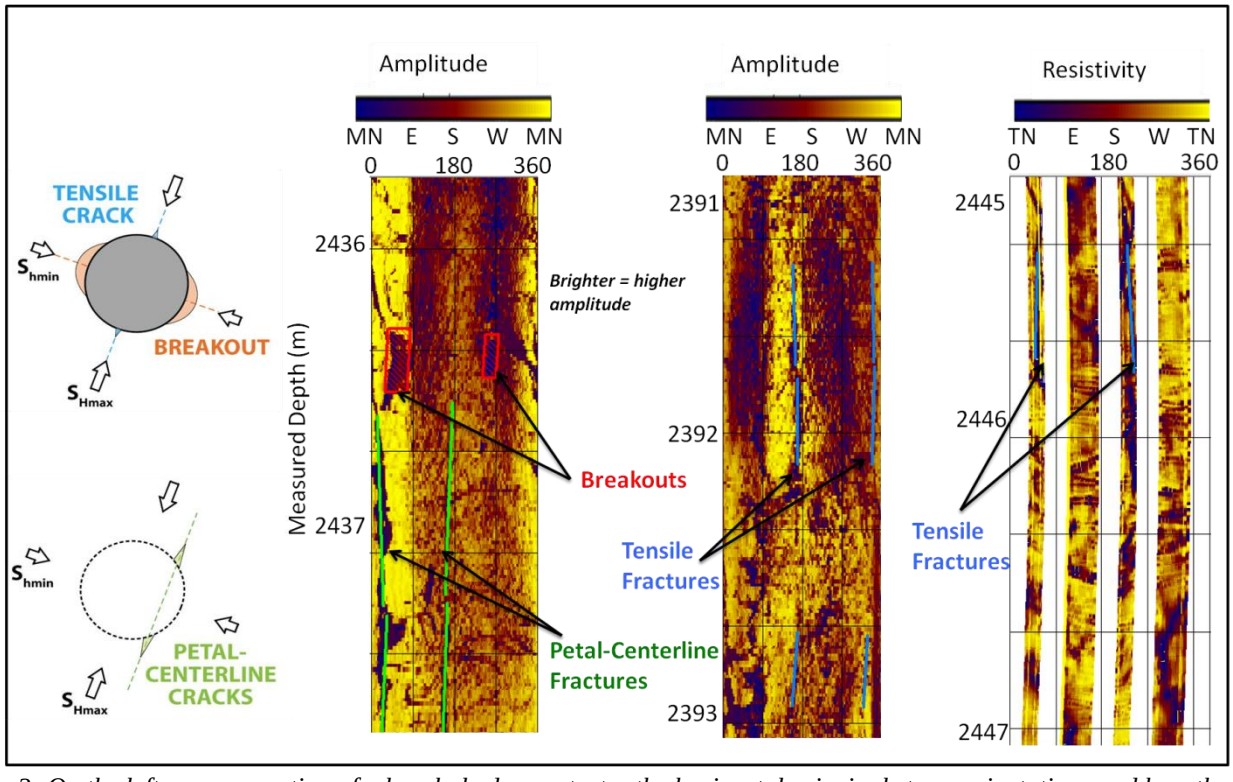

Figure 3: On the left, a cross section of a borehole demonstrates the horizontal principal stress orientations and how they relate to the borehole induced structures; tensile fractures, breakouts and petal-centerline fractures. In the three ABI85 and FMI image logs on the right of the figure, these deformations of the borehole wall are pointed out in the image.

This analysis assumes that one principal stress orientation is vertical, consistent with Andersonian tectonics. If the borehole deviations is up to 12-15 degrees, then the azimuth of breakouts are assumed to correspond with the azimuth of S_{hmin} and the azimuth of tensile fractures correspond with the azimuth of S_{Hmax} (Peska and Zoback, 1995) and the average of petal-centerline fracture orientations corresponds with S_{hmin} (Davatzes and Hickman, 2010; Garza-Cruz and Davatzes 2010). The analysis is restricted to the near-vertical segments of these boreholes.

The program WellCAD was used for the analysis of all the image logs in this study, which provides interpretation tools to identify and gather the attributes of natural fractures, foliation/bedding and borehole induced structures. The attributes of these features were then analyzed using Matlab scripts. The data gathered for natural fractures and bedding are apparent and true dip, dip azimuth, measured and true vertical depth, the type of structure and the quality of the structure picked. The data recorded for borehole induced structures are azimuth, width of structure, the height, measured and true vertical depth, the type of drilling induced structure and the quality. The quality criteria are the same utilized in Blake and Davatzes, 2012.

Principal horizontal stress direction

All of the image logs collected by the Navy GPO had borehole induced structures identified; the number of structures (i.e. the number of data points) greatly varied. This variance was dependent upon the quality of the image log itself, the length of the depth span imaged and the actual number of borehole deformation. Table 1 demonstrates how the calculated minimum horizontal principal stress orientation with one standard deviation for each borehole compares to the depth span of the data set, the number of data points and the change in principal stress orientation between locations.

Table 1: Description of the data sets used in this study and the calculated minimum horizontal principal stress.

Borehole Name	Site	Number of data points	Length Analyzed (meters)	Type of Image Log	S_{hmin} Orientation
66-8	Coso	151	1077	ABI85	087±46
FOH-3D	Fallon	608	806	FMI and ABI85	096±12
FLTH 88-24	Fallon	116	707	UBI	095±26
HWAD-2A	Hawthorne	236	1097	UBI	133±23
HWAD-3	Hawthorne	12	551	UBI	086±11
NAFEC-3	NAFEC	52	806	UBI	106±32
CMAGR 17-8	CMAGR	56	681	UBI	104±25

STRESS HETEROGENEITY

Spectral Analysis

The variation of the S_{hmin} orientation around the calculated mean direction defines a rotation of the horizontal principal stresses; these rotations can be characterized as superimposed sine waves with varying amplitudes and wavelengths. It is assumed that the orientation of the principal stresses rotate around a vertical axis and that the structures identified in the image log accurately provide the horizontal principal stress of the volume pierced by the borehole. The method used to determine how much each wavelength of the superimposed sine waves attributes to the changes in stress direction is called fractal analysis and the relative measure is referred to as the power spectral density, derived using a Fourier Transform (Hamming, 1989). By determining the frequency each wavelength contributes to the stress rotation, the scaling properties of stress heterogeneity from a vertical mean for the volume pierced by each borehole can be determined and demonstrate the length-scale sources of principal stress variation from the regional stress orientation.

Shamir and Zoback (1994), Day-Lewis et al. (2010),Valley and Evans (2010) and Blake and Davatzes (2011, 2012) have tested the length-scale dependence of the horizontal principal stresses on data sets using borehole induced structures as well. These previous analyses suggest that when the data is displayed as power-frequency in log-log space the data is linearly distributed and corresponds to frequency-magnitude distributions of earthquakes near the area intersected by the borehole (Shamir and Zoback, 1995; Day-Lewis et al., 2010; Blake and Davatzes, 2011, 2012). When stress data was compared in 4 boreholes proximal to the Coso geothermal field, the scaling relationship suggested that the variation in stress orientation changed due to proximity to the Coso Wash Fault, a normal fault that strikes through the field, as well as earthquakes in the nearby volume of rock (Blake and Davatzes, 2011).

Spectral analysis assumes that data is evenly spaced and the stress data collected from image logs is unevenly spaced, which meant that the data needed to be interpolated to be analyzed by two methods; Periodogram and Multitaper. For the third method used, the Autoregressive Moving Average Spectral Analysis (ARMASA) (See Blake and Davatzes, 2011), no interpolated is needed, the method uses an iterative interpolation and statistical testing to determine the power spectral density. These methods were tested on synthetic data sets in previous analysis to make sure that they can be applied to this type of stress data (Day Lewis et al., 2010; Blake and Davatzes, 2011).

The methods used in Blake and Davatzes, 2011 were applied in this analysis of stress heterogeneity, which included an analysis of similarly distributed colored noise for each data set to obtain an error estimate. The self-affine relationship of power spectral density and frequency is:

$$PSD = f^{\beta}$$

where PSD is the power spectral density (deg^2-m), f is the frequency (m^{-1}) and β is the spectral slope (deg^2-m)(m). In Table 2, the calculated spectral slope for each of the studied boreholes is given, along with the frequency span that the slope was calculated for.

Table 2: The calculated minimum horizontal principal stress, spectral slope and the frequency span that the spectral slope was calculated for each borehole.

Borehole Name	**S_{hmin} Orientation**	**Spectral Slope (deg^2m)(m)**	**Frequency Span (m^{-1})**
66-8	087±46	-2.61±0.35	$10^{-2.85}$ to $10^{-0.67}$
FOH-3D	096±12	-3.03±0.20	$10^{-2.4}$ to $10^{-1.35}$
FLTH 88-24	095±26	-2.53±0.02	$10^{-2.21}$ to $10^{-0.78}$
HWAD-2A	133±23	-3.75±0.14	$10^{-1.44}$ to $10^{-0.48}$
HWAD-3	086±11	-2.94±0.38	$10^{-2.03}$ to $10^{-0.44}$
NAFEC-3	106±32	-3.05±0.48	$10^{-2.47}$ to $10^{-0.71}$
CMAGR 17-8	104±25	-3.67±0.52	$10^{-1.79}$ to $10^{-0.42}$

DISCUSSION

Each of the Navy GPO exploration and development sites span different tectonic environments, the boreholes intersect many different lithologies, have different horizontal principal stress orientations and have different amounts of stress heterogeneity. The stress heterogeneity for each borehole is interpreted through the amount of standard deviation in the calculated vertical mean stress orientation and the spectral slope. The linear spectral slope demonstrates a fractal behavior (Turcotte, 1997) and, when assuming that the relationship is a self-affine fractal, a fractal dimension can be calculated using the spectral slope:

$$D_{rot} = \frac{5 - \beta}{2}$$

where D_{rot} is the fractal dimension of stress rotations (Turcotte, 1997). The values for each of the calculated spectral slopes are given in Table 3.

In this analysis, the sources of stress rotations tested were recent fracture slip and the intersected lithology (Scholz, 2002; Jaeger et al., 2007). Earthquakes proximal to each borehole were used to determine if the rotations of the principal stresses with depth were due to slip on faults (Day-Lewis et al., 2010). Earthquake frequency ($\log_{10}$) and magnitude also have a fractal distribution; a slope of this distribution can be calculated as (Shamir and Zoback, 1992; Day-Lewis et al., 2010; Blake and Davatzes, 2011, 2012):

$$D_{eq} = -\frac{bd}{q}$$

where b is the slope of the relationship between frequency ($\log_{10}$) and magnitude, d represents the shape of the fracture slipping, q is the moment magnitudes relationship to the magnitude of the earthquake and D_{eq} is the fractal dimension of earthquakes (Gutenberg and Richter, 1944; Kanamori and Anderson, 1975). The calculated earthquake fractal dimension proximal to each borehole is given in Table 3.

To test whether the variation in principal stress orientation with depth in each borehole was due to the changes in lithology, the same methodology used to derive the stress heterogeneity fractal dimension was used to determine a gamma ray fractal dimension. By analyzing the variation in gamma ray values over the same depth span of the imaged borehole using spectral analysis, the dependence of stress heterogeneity based on changes in lithology was tested. The results of this calculation are given in Table 3.

Table 3: Calculated minimum horizontal principal stress orientation with fractal dimensions of stress rotation, earthquake magnitude-frequency and gamma ray.

Borehole Name	S_{hmin} Orientation	D_{rot}	D_{eq}	D_{GR}
66-8	087±46	1.02-1.37	1.36-2.04	1.51-1.81
FOH-3D	096±12	0.89-1.09	1.39-2.08	1.56-1.67
FLTH 88-24	095±26	1.23-1.24	1.37-2.08	0.98-1.18
HWAD-2A	133±23	0.55-0.70	0.71-1.06	1.39-1.59
HWAD-3	086±11	0.84-1.22	1.32-1.49	1.93-2.00
NAFEC-3	106±32	0.74-1.22	2.71-4.06	1.71-1.84
CMAGR 17-8	104±25	0.41-0.93	2.72-4.08	1.10-1.66

The only overlap in the data from this analysis is from the Coso 66-8 stress and earthquake data. This coincides with

previous studies comparing these two data sets at the Coso geothermal field from Blake and Davatzes, 2011. This would suggest that the variation in stress orientation in Coso 66-8 is due to slip on fractures near the volume pierced by the borehole. The other borehole earthquake data does not overlap with the stress data, suggesting that the variation in stress orientation with depth is not due to slip on proximal earthquakes. However, a large difference between the earthquake datasets was the microseismic earthquake catalog from the Navy GPO for the Coso field and the less site specific data from the Southern California Earthquake Catalog and from the USGS, which would suggest that if there were similar data sets, these data could overlap.

The lack of overlap between the stress heterogeneity fractal dimension and the gamma ray fractal dimension suggests that the lithology in each of the boreholes does not control the changes in principal stress orientation. This result is not surprising in the boreholes which intersect mostly crystalline rock (Coso 66-8, HWAD-2A, NAFEC-3 and CMAGR 17-8) but is a surprising result for the two holes at NAS Fallon and HWAD-3, which intersect mostly alluvium, lake bed sediments and/or volcanic sediments. There are other sources of stress heterogeneity that have not been tested for in these data sets including proximity to large faults, topography and other elastic properties of the rocks (Zoback, 2007; Zang and Stephansson, 2010).

For all of the studied boreholes, the occurrence of stress heterogeneity does suggest active areas of crustal movement for the exploration sites. The boreholes with greater amounts of stress heterogeneity with depth would suggest that there are a greater number of fractures optimally oriented for fluid movement through a potential geothermal system. The borehole with the least potential based on down hole temperatures and lack of open fractures, HWAD-3, also happens to have to smallest standard deviation in stress orientation. A similar result was seen in the image log data from the Coso geothermal field; the studied boreholes inside the field had a greater amount of stress heterogeneity (standard deviation) then on the margins of the field (Blake and Davatzes, 2011). Even though FOH-3D and FLTH 88-24 have nearly the same S_{hmin} orientation, they do have very different stress heterogeneity (standard deviation). The Navy GPO already has a great amount of data on FOH-3D, but within the next few months will be performing a flow test on FLTH 88-24; the results of this test could demonstrate the applicability of stress heterogeneity as a useful geothermal exploration tool.

CONCLUSION

The boreholes drilled for exploration by the Navy GPO demonstrate a great amount of stress heterogeneity but the reason for this variation in stress with depth is still not obvious for most sites. The borehole induced structures identified in image logs from exploration boreholes and a borehole from the Coso geothermal field were used to determine the orientation of the minimum horizontal principal stress, the standard deviation in stress orientation and the stress rotation fractal dimension calculated using fractal statistics to better understand stress heterogeneity. In the developed geothermal system, Coso, the stress heterogeneity seems to coincide with slip of faults based on the overlap of fractal dimensions of stress rotations and earthquake magnitude-frequency data. The results from analysis of Coso 66-8 demonstrate this overlap, as well as previous analysis of four more boreholes in the Coso geothermal field (Blake and Davatzes, 2011). However, the lack of overlap of the remaining exploration sites with earthquake data may be due a robust microseismic data set for the Coso field with no similar dataset for the other sites. A comparison of stress heterogeneity to gamma ray data, as a measure of the variation in lithology with depth in each of the boreholes, did not demonstrate any fractal dimension overlap suggesting that lithology is not controlling the variation in stress for these exploration boreholes. Other sources of horizontal principal stress heterogeneity have yet to be tested including topography, elastic properties of the intersected rocks and proximity to large stress controlling faults. The amount of stress heterogeneity with depth in the studied boreholes does suggest that the greater the stress heterogeneity, the more fractures available for opening, permeability and fluid flow, the more prospective a geothermal test hole may be.

Acknowledgements

I would like to thank all of my past and current co-workers at the Navy GPO for all they have taught me, as well as their support and help the last 18 months. Special thanks to Nick Davatzes for his continued guidance, help and friendship. Also, thank you to Jess McCoullough and the Coso Operating Company for the 66-8 data and the continuous learning experience.

REFERENCES

Adams, M.C., Moore, J.N., Bjornstad, S., and Norman, D.I. (2000). Geologist History of the Coso geothermal field. *Proceedings World Geothermal Congress 2000, Kyushu-Tohoku, Japan, May 28-June 10, 2000*, 2463-2469.

Alm, S., Bjornstad, S., Lazaro, M., Sabin, A., Meade, D., Shoffner, J., Huang, W.C., Unruh, J., Strane, M. and Ross, H. (2010). Geothermal Energy Resource Investigations, Chocolate Mountains Aerial Gunnery Range, Imperial Valley, California, *Geothermal Resource Council*.

Barton, C.A., Hickman, S., Morin, R., Zoback, M.D., Finkbeiner, T., Sass, J. and Benoit, D. (1997), Fracture Permeability and its Relationship to In-Situ Stress in the Dixie Valley, Nevada, Geothermal Reservoir, *Proceedings Twenty-Second Stanford University Geothermal Workshop*.

Barton, C.A., Castillo, D.A., Moos, D., Peska, P. and Zoback, M.D. (1998), Characterizing the full stress tensor based on observations of drilling-induced wellbore failures in vertical and inclined boreholes leading to improved wellbore stability and permeability prediction,*APPEA* Journal, 29-53.

Barton, C.A. and Zoback, M.D. (2002), Wellbore imaging technologies applied to reservoir geomechanics and environmental engineering, *AAPG Methods in Exploration*, **13**, 229-239.

Bellier, O. and Zoback, M.L., (1995), ―ecent state of stress change in the Walker Lane zone, western Basin and Range province, United States,*Tectonics*, **14(3)**, 564-593.

Bennett, R. A., B. P. Wernicke, N. A. Niemi, A. M. Friedrich, and J. L. Davis (2003), "Contemporary strain rates in the northern Basin and Range province from GPS data," *Tectonics*, **22(2)**, 1008, doi:10.1029/ 2001TC001355.

Bjornstad, S., Hall, B., Unruh, J. and Richards-Dinger, K. (2006). Geothermal Resource Exploration, NAF El Centro-Superstition Mountain Area, Imperial Valley, California, *Geothermal Resource Council.*

Blake, K. and Davatzes, N.C. (2011), "Crustal Stress Heterogeneity in the Vinicity of Coso Geothermal Field, CA," *Proceedings Thirty-Seventh Stanford University Geothermal Workshop*.

Blake, K. and Davatzes, N.C. (2012), "Borehole Image Log and Statistical Analysis of FOH-3D, Fallon Naval Air Station, NV", *Proceedings Thirty-Eight Stanford University Geothermal Workshop*.

Blewitt, G., Hammond, W.C., and Kreemer, C. (2009), ―Geodetic observation of contemporary deformation in the northern Walker Lane: 1. Semipermanent GPS strategy,*Geological Society of America Special Paper*, 1-15.

Brie, A., Codazzi, C., Denoo, S., Mueller and M., Plona, T. (1998). New Directions in Sonic Logging, *Oilfield Review*, Spring.

Crowe, B.M. (1978). Cenozoic volcanic geology and probable age of inception of basin-range faulting in the southeasternmost Chocolate Mountains, California, *Geol. Soc. Am. Bull*., **89**, 251-264.

Curewitz, D., and J. A. Karson,(1997), "Structural settings of hydrothermal outflow: Fracture permeability maintained by fault propagation and interaction," *J. Volcanol. Geotherm. Res.*, **79**, 149–168.

Davatzes, N.C. and Hickman, S. (2006), Stress and faulting in the Coso Geothermal Field: Update and recent results from the East Flank and Coso Wash,*Proceedings Thirty-First Stanford University Geothermal Workshop*.

Davatzes, N.C. and Hickman, S. (2009), ―Stress, fracture, and fluid-flow analysis using acoustic and electrical image logs in hot fractures granites of the Coso Geothermal Field, California,‖ *AAPG Memoir*, **92**, 1-35.

Davatzes, N.C. and Hickman,S. (2010), The feedback between stress, faulting, and fluid flow: Lessons from the Coso Geothermal Field, CA, USA,*Proceedings World Geothermal Congress*, 1-14.

Davatzes, N.C. and Hickman, S. (2011), Natural Fractures, Mechanical Properties, and In-Situ Stress in the Planning and Execution of the Desert Peak EGS Experiment, *Proceedings AAPG/SPE/SEG Hedberg Conference*.

Day-Lewis, A., Zoback, M.D. and Hickman, S. (2010), Scale invariant stress orientations and seismicity rates near the San Andreas Fault, *Geophysical Research Letters*, **37**, L24304, doi: 10.1029/2010FLO45025

Eaton, G.P. (1982), The Basin and Range Province: Origin and Tectonic Signifance, *Ann. Rev. Earth and Planetary Science*, **10**, 409-440.

Ekstrom, M.P., Dahan, C, Chen, M.-Y., Lloyd, P., and Rossi, D.J., (1987), Formation imaging with microelectrical scanning arrays, *Log Analyst*, **28**, 294-306.

Faulds, J.E., Coolbaugh, M.F., Vice, G.S., and Edwards, M.L. (2006), Characterizing Structural Controls of Geothermal Fields in the Northwestern Great Basin: A Progress Report, *Geothermal Resources Council Transactions,* **30,** 69-76.

Fialko, Y. and Simons, M. (2000). Deformation and seismicity in the Coso geothermal area, Inyo County, California: Observations and modeling using satellite radar interferometry, *J. of Geophys. Research*, **105**, 781-21, 794.

Garza-Cruz, T. and Davatzes, N.C. (2010), Numerical Modeling of the Nucleation Conditions of Petal-Centerline Fractures Below a Borehole Floow, A Sensitivity Study and Application to the Coso Geothermal Field, *Geothermal Resource Council*.

Hamming, R. W. (1989), *Numerical Methods for Scientists and Engineers*, Dover Publications, Inc. New York, NY, 503-516.

Heidbach, O., Tingay, M., Barth, A., Reinecker, J., Kurfeß, D. and M**ü**ller, B. (2010), Global crustal stress pattern based on the World Stress Map database release 2008, *Tectonophysics*, **482**, 3-15.

Hickman, S., Zoback, M.D., Barton, C., Benoit, R., Svitek, J. and Summers, R. (2002), Stress and permeability heterogeneity within the Dixie Valley geothermal reservoir: Recent results from well 82-5, *Proceedings Stanford University Geothermal Workshop*.

Hill, D. P. (1971), Velocity Gradients and Anelasticity from Crustal Body Wave Amplitudes, *Journal of Geophysical Research*, **76**, 3309-3325.

Jaeger, J.C., Cook, N.G. and Zimmerman, R.W. (2007), *Fundamentals of Rock Mechanics*. 4. 1. Malden, MA: Blackwell Publishing, 1-7.

Kanamori, H., and Anderson, D.L. (1975), Theoretical basis of some empirical relations in seismology, *Bulletin Seismological Society of America*, **65**, 1073-1095.

Katzenstein, A.M. and Bjornstad, S.C. (1987), Geothermal Resource Evaluation at Naval Air Station Fallon, Nevada, Naval Weapons Center Technical Publication 6808.

Katzenstein, A., Bjornstad, S., and Meade, D. (2002). Geothermal Resource Evaluation of the Hawthorne Army Depot (HWAD), Hawthorne, NV. *Technical Paper for the Navy Geothermal Program Office*.

Kovac, K.M., Moore, J.N., and Lutz, S.J. (2005). Geological framework of the East Flank, Coso geothermal field: Implications for EGS development, *Proceedings Geothermal Reservoir Engineering, Stanford, CA SGP-TR-176*, 7.

Kremer, C., G. Blewitt, and W. C. Hammond (2009), Geodetic Transition on contemporary deformation in the northern Walker Lane: 2, velocity and tensor strain rate analysis, Late Cenozoic Structure and Evolution of the Great Basin – Sierra Nevada, Special Paper 447, doi: 10.1130/2009.2447(02).

Kremer, C., Blewitt, G., and Hammond, W.C. (2010), Evidence for an active shear zone in southern Nevada linking the Wasatch fault to the Eastern California shear zone, *Geology*, **38**, 475-478.

Lazaro, M., Alm, S., Tiedeman, A., Page, C., Meade, D., Shoffner, J., and Bucher, K. (2011), Department of the Navy Geothermal Exploration on Naval Air Station Fall (NASF) Managed Lands in Dixie Valley, Nevada, *Geothermal Resource Council Transactions 2011*.

Li, Y. and Schmidt, D.R. (1999), Well-bore bottom stress concentration and induced core fractures, *AAPG Bulletin*, **81**, 1909-1925.

Lin, J. and Stein, R.S. (2004). Stress triggering in thrust and subduction earthquakes and stress interaction between the southern San Andreas and nearby thrust and strik-slip faults, *J. of Geophys. Research*, **107**, p.1-19.

Manley, C.R. and Bacon, C.R. (2001). Rhyolite thermobarometry and the shallowing of the magma reservoir, Coso Volcanic Field, California, *J. of Petrology*, **41**, p.149-174.

Moeck, I., Hinz, J., Faulds, J., Bell, J., Kell-Hills, A. (2010). 3D geological mapping as a new method in geothermal exploration: A case study from central Nevada, *Geothermal Resource Council*.

Monastero, F.C., Katzenstein, A.M., Miller, S.J., Unruh, J.R., Adams, M.C. and Richards-Dinger, K. (2005). The Coso geothermal field: A nascent Metamorphic core complex. *Geo.Soc. of Am Bul.*, **177(11/12)**, 1534-1553.

Peska, P. and Zoback, M.D. (1995), Compressive and tensile failure of inclined well bores and determination of in situ stress and rock strength,*J.of Geophys. Research*, **100**, 27911-12811.

Scholz, C. (2002), *The Mechanics of Earthquakes and Faulting*, 2. 1. New York, NY: Cambridge, p. 174-243.

Shamir, G., and Zoback, M.D. (1992). Stress orientation profile to 3.5 km depth near the San
Andreas fault at Cajon Pass, California: *J. of Geophys. Research*, **97**, 5059-5080.

Shearer, P., Hauksson, E., and Lin, G., (2005). Southern California Hypocenter Relocation with Waveform Cross-Correlation, Part 2: Results using Source-Specific Station Terms and Cluster Analysis, *Bulletin of the Seismological Society of America*, v. 95, n. 3, p. 904-915.

Shoffner, J., Li, Y, Hinz, N., Sabin, A., Lazaro, M. and Alm, S. (2010). Understanding Fault Characteristics and Sediment Depth for Geothermal Exploration Using 3D Gravity Inversion In Walker Valley, Nevada, *Geothermal Resource Council*.

Turcotte, D.L. (1997), *Fractals and Chaos in Geology and Geophysics*, 2.1. New York, NY: Cambridge, pg. 56-79.

Unruh, J.R. and Steig, A.R. (2004). Mapping and characterization of neotectonic structures in a releasing stepover, northing Coso Range, eartern Califonia, *Final technical report submitted to the U.S. Navy Geothermal Progream Office*, China Lake Naval Air Warefare Center, Contract N68936-02-C-0208, p.46.

Valley, B. and Evans, K.R. (2010), Stress Heterogeneity in the Granite of the Soultz EGS Reservoir Inferred from Analysis of Wellbore Failure, *Proceedings World Geothermal Congress 2010*, Bali, Indonesia.

Wicks, C.W., Thatcher, W., Monastero, F.C. and Hasting, M.A. (2001). Steady-state
deformation of the Coso Range, east-central California, inferred from satellite radar interferometry, *J. of Geophys. Research*, v. 106, no. B7, p. 13,769-13,780.

Willis, G.F. and Tosdal, R.M. (1992). Formation of gold veins and breccias during dextral strike-slip faulting in the Mesquite mining district, southeastern California, *Economic Geology*.

World Stress Map (2008), http://www.world-stress-map.org.

Zang, A. and Stephansson, O. (2010). *Stress Field of the Earth's Crust*, Springer, Dordrecht, **322**, 231-243.

Zemanek, J., Glenn, E.E., Norton, I.J., Caldwell, R.L. (1970). Formation evaluation by inspection with the borehole televiewer, *Geophysics*, v. 35, n. 2, p. 254-269.

Zoback, M.D., Moos, D., Mastin, L. and Anderson, R.N. (1985), Wellbore breakouts and in-situ stress, Journal of Geophysical Research, **90**, 5,523-5,530.

Zoback, M.D. (2007). *Reservoir Geomechanics*: Cambridge, New York, NY. Print.

Zoback, M.L., Zoback, M.D., Adams, J., Assumpcão, M., Bell, S., Bergman, E.A., Blümling, P., Brereton, N.R., Denham, D., Ding, J., Fuchs, K., Gay, N., Gregersen, S., Gupta, H.K., Gvishiani, A., Jacov, K., Klein, R., Knoll, P., Magee, M., Mercier, J.L., Müller, B.C., Paquin, C., Rajendran, K., Stephansson, O., Suarez, G., Suter, M., Udias, A., Xu, Z. H. and Zhizhin, M. (1989), Global patterns of tectonic stress, *Nature*, **341**, 291-298.

Zoback, M.L. (1989), State of Stress and Modern Deformation of the Northern Basin and Range Province, *Journal of Geophysical Research*, **94(B6)**, 7105-712.